Methods for Speed Sensorless Control of AC Drives

Joachim Holtz, *Fellow*, IEEE
University of Wuppertal – Germany

Abstract — **The operation of speed controlled ac drives without mechanical speed or position sensors requires the estimation of internal state variables of the machine. The assessment is based exclusively on measured terminal voltages and currents. Low cost, medium performance sensorless drives can be designed using simple algebraic speed estimators. High-performance systems rely on dynamic models for the estimation of the magnitude and spatial orientation of magnetic flux waves in the stator or in the rotor. Open loop estimators and closed loop observers differ with respect to accuracy, robustness, and limits of applicability. The overview in this paper uses signal flow graphs of complex space vector quantities to give an insightful description of the physical and mathematical systems used in sensorless ac drive control.**

I. Introduction

AC drives based on full digital control have reached the status of a maturing technology in a broad range of applications ranging from low-cost to high-performance systems. Continuing research has concentrated on the elimination of the speed sensor at the machine shaft without deteriorating the dynamic performance of the drive control system. Speed estimation is an issue of particular interest with induction motor drives where the mechanical speed of the rotor is generally different from the speed of the revolving magnetic field. The advantages of speed sensorless induction motor drives are lower cost, reduced size of the drive machine, elimination of the sensor cable, and increased reliability. A variety of different solutions for sensorless ac drives have been proposed in the past few years. This paper reviews their merits and limits based on a survey of the available literature.

II. Machine Dynamics

2.1 Basic equations

The graphic representation of dynamic systems by signal flow diagrams is a well-established tool. Its extension to complex state variables, describing the sinusoidal distribution of the magnetic and electrical quantities around the circular air gap of a rotating machine has been recently proposed [1]. This technique offers the advantage of conveying information on the dynamic behavior of a system of considerable complexity in an easy-to-understand symbolic notation.

The machine equations in terms of complex space vector quantities are

$$\boldsymbol{u}_\mathrm{s} = r_\mathrm{s}\boldsymbol{i}_\mathrm{s} + \frac{d\boldsymbol{\psi}_\mathrm{s}}{d\tau} + \mathrm{j}\omega_\mathrm{k}\boldsymbol{\psi}_\mathrm{s} \tag{1a}$$

$$0 = r_\mathrm{r}\boldsymbol{i}_\mathrm{r} + \frac{d\boldsymbol{\psi}_\mathrm{r}}{d\tau} + \mathrm{j}(\omega_\mathrm{k} - \omega)\boldsymbol{\psi}_\mathrm{r}, \tag{1b}$$

where ω_k is the angular velocity of the reference frame, and ω is the angular velocity of the rotor. The flux linkage equations are

$$\boldsymbol{\psi}_\mathrm{s} = l_\mathrm{s}\boldsymbol{i}_\mathrm{s} + l_\mathrm{h}\boldsymbol{i}_\mathrm{r} \tag{2a}$$

$$\boldsymbol{\psi}_\mathrm{r} = l_\mathrm{h}\boldsymbol{i}_\mathrm{s} + l_\mathrm{r}\boldsymbol{i}_\mathrm{r}. \tag{2b}$$

The electromagnetic torque is proportional to the z-component of the external product of two state variable space vectors, e. g. $|\boldsymbol{\psi}_\mathrm{s} \times \boldsymbol{i}_\mathrm{s}|_\mathrm{z}$. This expression forms the link to the dynamics of the mechanical system,

$$\tau_\mathrm{m}\frac{d\omega}{d\tau} = |\boldsymbol{\psi}_\mathrm{s} \times \boldsymbol{i}_\mathrm{s}|_\mathrm{z} - T_\mathrm{L}, \tag{3}$$

where τ_m is the normalized mechanical time constant, and T_L is the load torque. Note that time is normalized: $\tau = \omega_\mathrm{sR} t$, where ω_sR is the rated stator frequency.

At least one, in the general case both machine windings see the common reference frame rotating, depending on the choice of ω_k.

2.2 The complex signal flow diagram

The machine equations depend on the respective space vectors that are chosen as state variables. Choosing the stator current vector and the rotor flux vector as state variables converts the machine equations to

$$\tau_\sigma{}'\frac{d\boldsymbol{i}_\mathrm{s}}{d\tau} + \boldsymbol{i}_\mathrm{s} = -\mathrm{j}\omega_\mathrm{k}\tau_\sigma{}'\boldsymbol{i}_\mathrm{s} + \frac{k_\mathrm{r}}{r_\sigma\,\tau_\mathrm{r}}(1 - \mathrm{j}\,\omega\,\tau_\mathrm{r})\;\boldsymbol{\psi}_\mathrm{r} + \frac{1}{r_\sigma}\boldsymbol{u}_\mathrm{s} \tag{4a}$$

$$\tau_\mathrm{r}\frac{d\boldsymbol{\psi}_\mathrm{r}}{d\tau} + \boldsymbol{\psi}_\mathrm{r} = -\mathrm{j}(\omega_\mathrm{k} - \omega)\tau_\mathrm{r}\boldsymbol{\psi}_\mathrm{r} + l_\mathrm{h}\boldsymbol{i}_\mathrm{s}, \tag{4b}$$

which follows from (1) and (2). The coefficients in (4) are $\tau_\sigma{}' = \sigma l_\mathrm{s}/r_\sigma$, $r_\sigma = r_\mathrm{s} + k_\mathrm{r}^2\, r_\mathrm{r}$, and $k_\mathrm{r} = l_\mathrm{h}/l_\mathrm{r}$, where $\tau_\mathrm{r} = l_\mathrm{r}/r_\mathrm{r}$ is the rotor time constant, and $\sigma = 1 - k_\mathrm{s}\,k_\mathrm{r}$ is the total leakage coefficient.

The graphic interpretation of (4) is the signal flow dia-

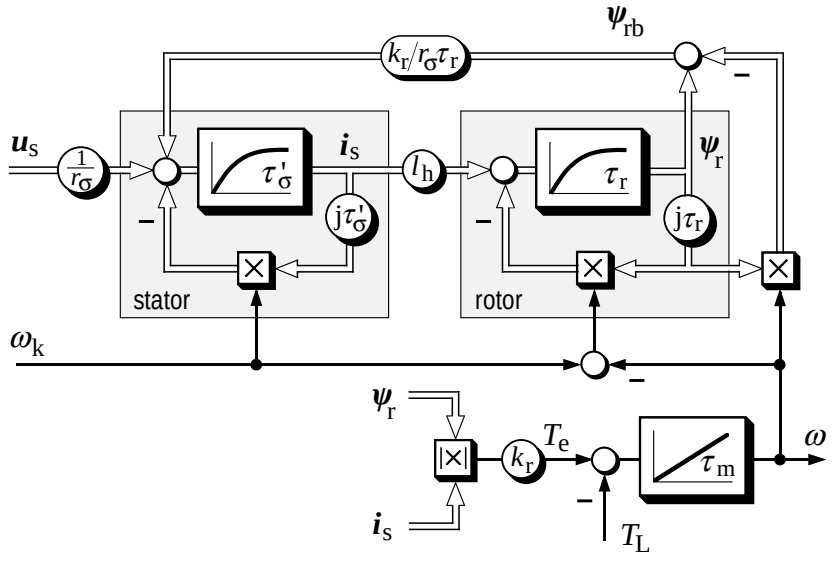

Fig.1: Complex signal flow diagram of the induction motor, state variables: stator current, rotor flux

Published in K. Rajashekara (Editor) „Sensorless Control of AC Motors". IEEE Press Book, 1996.

gram Fig. 1. This graph exhibits two fundamental structures, one on the left-hand side which represents the stator winding, and one on the right-hand side representing the rotor winding. Each winding is characterized by a first-order delay element and a normalized time constant. The time constant reappears as an imaginary factor in the internal feedback path of the respective winding structure, describing the cross-coupling between orthogonal space vector components of the output to the input. The ω-multiplicator determines the angular velocity at which the respective winding rotates against the ω_k-reference frame [1].

Equations (3) and (2b) serve to derive the electromagnetic torque $T_e = k_r \cdot |\boldsymbol{\psi}_r \times \boldsymbol{i}_s|_z$ from the actual state variables. The result is represented in the lower portion of the graph.

III. Limitations

The system in Fig. 1 is now considered for the special case of operation at very low stator frequency, $\omega_s \to 0$. The following equation can be directly read from the signal flow diagram:

$$\tilde{\boldsymbol{\psi}}_r = \frac{l_h}{\tau_r s + 1 + j(\omega_k - \omega)\tau_r}\, \tilde{\boldsymbol{i}}_s, \tag{5}$$

where $\tilde{\boldsymbol{\psi}}_r$ and $\tilde{\boldsymbol{i}}_s$ are the Laplace transforms of the respective space vectors.

The feedback signal that acts from the rotor to the stator in Fig. 1 is composed of two components. The signal can be expressed as $\boldsymbol{\psi}_{rb} = \boldsymbol{\psi}_r (1 - j\omega\tau_r)$, and its Laplace transform is obtained with reference to (5):

$$\tilde{\boldsymbol{\psi}}_{rb} = l_h \frac{1 - j\omega\tau_r}{\tau_r s + 1 + j(\omega_k - \omega)\tau_r}\, \tilde{\boldsymbol{i}}_s. \tag{6}$$

As ω_s approaches zero, the feeding voltage vector $\boldsymbol{u}_s$ approaches zero frequency when observed in the stationary reference frame, $\omega_k = 0$. As a consequence, all steady-state signals tend to assume zero frequency, and the Laplace variable $s \to 0$. Hence we have from (6)

$$\lim_{s \to 0} \tilde{\boldsymbol{\psi}}_{rb} = \frac{l_h k_r}{r_\sigma \tau_r} \cdot \tilde{\boldsymbol{i}}_s \tag{7}$$

since the aforementioned two components of $\boldsymbol{\psi}_{rb}$ cancel. The right-hand side of (7) is independent of ω, indicating that, at zero stator frequency, variations of the mechanical angular velocity ω the rotor exert no influence on the stator. Particularly, they do not reflect on the stator current as the important measureable quantity for speed identification. Hence the mechanical speed of the rotor is not observable at $\omega_s = 0$.

The situation is different when operating near zero stator frequency. The aforementioned steady-state signals are now low frequency ac signals which get modified in phase angle and magnitude when passing through the τ_r-delay element on the right-hand side of Fig. 1. Hence, the cancellation of the two components of $\boldsymbol{\psi}_{rb}$ is not perfect. Particularly at higher speed is a voltage of substantial magnitude induced from the rotor in the stator. Its influence on measurable quantities at the machine terminals can be detected: the rotor state variables are then observable.

To reduce the influence of parameter mismatch and noise to a acceptable level, the stator frequency must be raised from zero to a minimum value. The unability to operate below this level constitutes a basic limitation for sensorless control.

IV. Drives for Moderate Dynamic Requirements

4.1 Back-emf based estimation

Pioneering work in sensorless vector control was contributed by *Joetten* [2]. His concept uses an estimated back emf vector $\boldsymbol{u}_i$ as the key signal from which the stator voltage reference and an estimated rotor frequency signal are generated. To this aim. the electromagnetic torque is expressed as

$$T_e = -|\boldsymbol{\psi}_r \times \boldsymbol{i}_r|_z = k_r \cdot |\boldsymbol{\psi}_r \times \boldsymbol{i}_s|_z . \tag{8}$$

Referring to stator coordinates, $\omega_k = 0$, the rotor current vector in this equation is substituted from (1b). It is further assumed that the rotor flux magnitude changes only slowly. The back-emf can be then approximated as

$$\boldsymbol{u}_i = \frac{d\boldsymbol{\psi}_r}{d\tau} \approx j\omega_s \boldsymbol{\psi}_r \tag{9}$$

which, after some cumputations, leads to

$$\omega_r = k_r r_r \frac{|\boldsymbol{\psi}_r \times \boldsymbol{i}_s|_z}{\boldsymbol{\psi}_{r\alpha}^2 + \boldsymbol{\psi}_{r\beta}^2}. \tag{10}$$

The rotor flux terms are replaced by $\boldsymbol{u}_i$ using (9):

$$\hat{\omega}_r = k_r r_r \omega_s \frac{\boldsymbol{u}_i \circ \boldsymbol{i}_s}{\boldsymbol{u}_i^2}. \tag{11}$$

This equation determines the signal flow graph Fig. 2, in which $\boldsymbol{u}_i$ is reconstructed with reference to (1a), (2) and (9)

$$\boldsymbol{u}_i = \boldsymbol{u}_s - r_s \boldsymbol{i}_s - \sigma l_s \frac{d\boldsymbol{i}_s}{d\tau} . \tag{12}$$

The rotor frequency estimator Fig. 2 forms part of the drive control system Fig. 3. The speed control loop is linearized by $1/\boldsymbol{\psi}_r^*$ for operation at field weakening. The torque reference signal T_e^* is limited in magnitude to prevent overload. This signal and the rotor flux magnitude determine the rotor frequency reference ω_r^*. A slip controller generates the stator frequency signal, which is used for field weakening control and field orientation, and in addition to determine the estimated speed $\hat{\omega}$. The estimated rotor frequency enters here after low pass filtering to avoid stability problems [2].

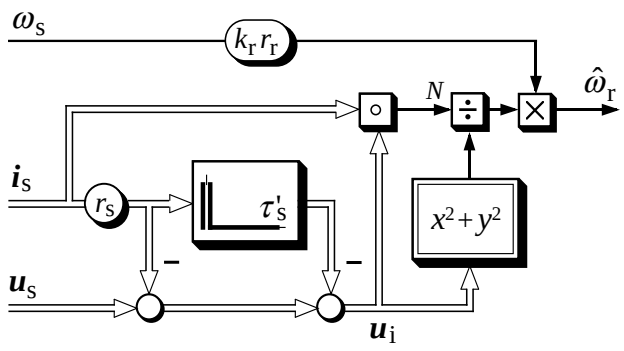

Fig. 2: Rotor frequency estimator based on the back emf vector $\boldsymbol{u}_i$; ***N*:** numerator

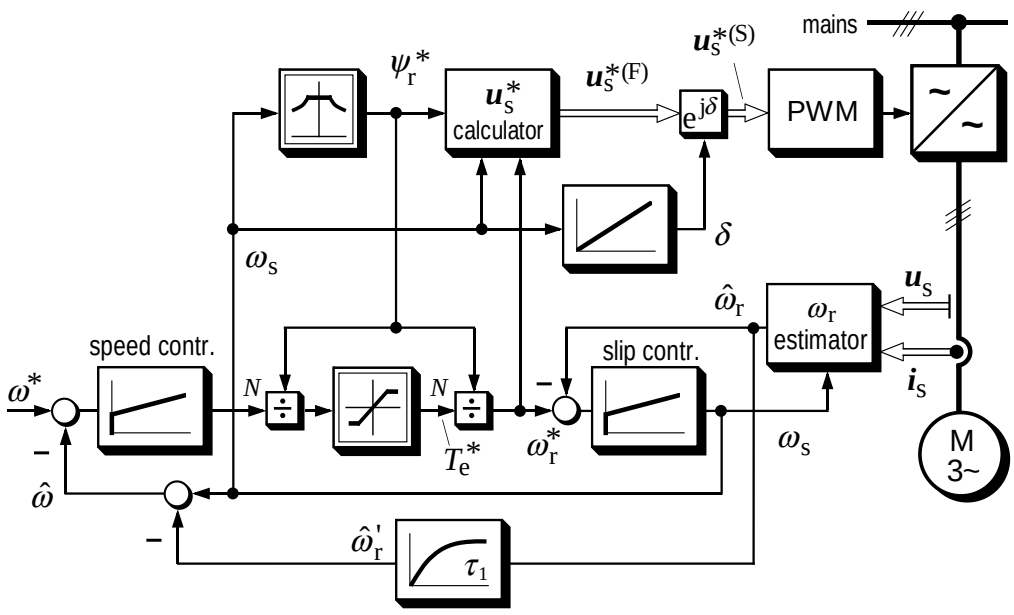

Fig. 3: Drive control system using the ω_r estimator of Fig. 4

The stator voltage reference $\boldsymbol{u}_s{}^{*(F)}$ is computed in field coordinates (superscript F). Its magnitude depends on ω_s and $\psi_r{}^*$, according to the programmed volts-per-hertz characteristic of the machine. $\omega_r{}^*$ controls the phase angle between $\boldsymbol{u}_s{}^*$ and $\boldsymbol{u}_i$, while $\boldsymbol{u}_i = j{\cdot}u_i$ defines the imaginary axis of the rotating reference frame.

The dynamic performance of this sensorless drive system is moderate, owing to a low-pass filter τ_1 in the feedback path of the speed loop. The filter eliminates the residual ripple content of the estimated slip. Torque rise time is around 40 ms. Dynamic control is satisfactory above 3 ... 5 % of rated speed.

4.2 Constant volts-per-hertz control

Low-cost sensorless drives have simple control structures suited for general purpose applications. Although being based on the simple volts-per-hertz characteristic of the machine, improved dynamic performance is achieved by an adequate design of the superimposed control structure as shown in Fig. 4, [3].

The machine dynamics are represented here in terms of the state variables $\boldsymbol{\psi}_s$ and $\boldsymbol{\psi}_r$. The system equations are derived from (1) and (2) in the stationary reference frame, $\omega_k = 0$, as

$$\frac{d\boldsymbol{\psi}_s}{d\tau} = \boldsymbol{u}_s - r_s \frac{1}{\sigma l_s}(\boldsymbol{\psi}_s - k_r \boldsymbol{\psi}_r) \qquad (13a)$$

$$\tau_r' \frac{d\boldsymbol{\psi}_r}{d\tau} + \boldsymbol{\psi}_r = -j\omega\tau_r' \boldsymbol{\psi}_r + k_s \boldsymbol{\psi}_s, \qquad (13b)$$

where $\tau_r' = \sigma l_r / r_r$. The corresponding signal flow graph on the right-hand side of Fig. 4 shows that the stator flux vector is generated as the integral of $\boldsymbol{u}_s - r_s{\cdot}\boldsymbol{i}_s$, where

$$\boldsymbol{i}_s = \frac{1}{\sigma l_s}(\boldsymbol{\psi}_s - k_r \boldsymbol{\psi}_r). \qquad (14)$$

The normalized time constant of the integrator is unity.

The key quantity of this control concept is the active stator current i_{sp}, computed as

$$i_{sp} = \frac{\boldsymbol{i}_s \circ \boldsymbol{u}_s}{u_s} = i_{s\alpha} \cos\vartheta + i_{s\beta} \sin\vartheta \qquad (15)$$

from the measured stator current and the phase angle ϑ of the stator voltage reference vector $\boldsymbol{u}_s{}^* = u_s{}^* e^{j\vartheta}$. The active stator current expresses torque in the base speed range and hence is represented by the output of the speed controller. Speed estimation is based on the stator frequency signal ω_s and the active stator current, which is proportional to the rotor frequency ω_r. An inner loop controls the active stator current, having its reference signal limited to prevent overload and pull-out. Fig. 4 shows that the external $\boldsymbol{i}_s{\cdot}r_s$ compensation eliminates the internal resistive voltage drop. This makes the trajectory of the stator flux vector independent of the stator current and the load. It provides a favorable dynamic behaviour of the machine and eliminates the need for the usual acceleration limiter in the speed reference channel. The torque rise time is around 10 ms, [3], which matches the dynamic performance of a thyristor converter controlled dc drive.

4.3 Speed estimation based on space harmonics

Secondary effects of the machine magnetics offer a potentiality for speed estimation. *Zinger et al.* [4] exploit rotor slot harmonics in the airgap field, which modulate the stator flux linkage with a frequency proportional to the rotor speed. The corresponding components of the induced voltage are separated from the resistive voltage drop by sensing at specially placed stator winding taps.

On condition that the number of rotor slots is not a multiple of three, which is true for most machines, the desired slot harmonic signals can be separated from the much larger fundamental emf by taking the sum of the three phase voltages in a wye connected winding. This eliminates all nontriplen voltage components, including the fundamental, while the slot harmonic voltages add up. Their frequency is a multiple of the mechanical rotor speed. Harmonic components other than the slot harmonics are suppressed by an adaptive bandpass filter, the center frequency of which is made to track the slot harmonic frequency using a phase locked loop (PLL). The speed signal is obtained from the output of the PLL.

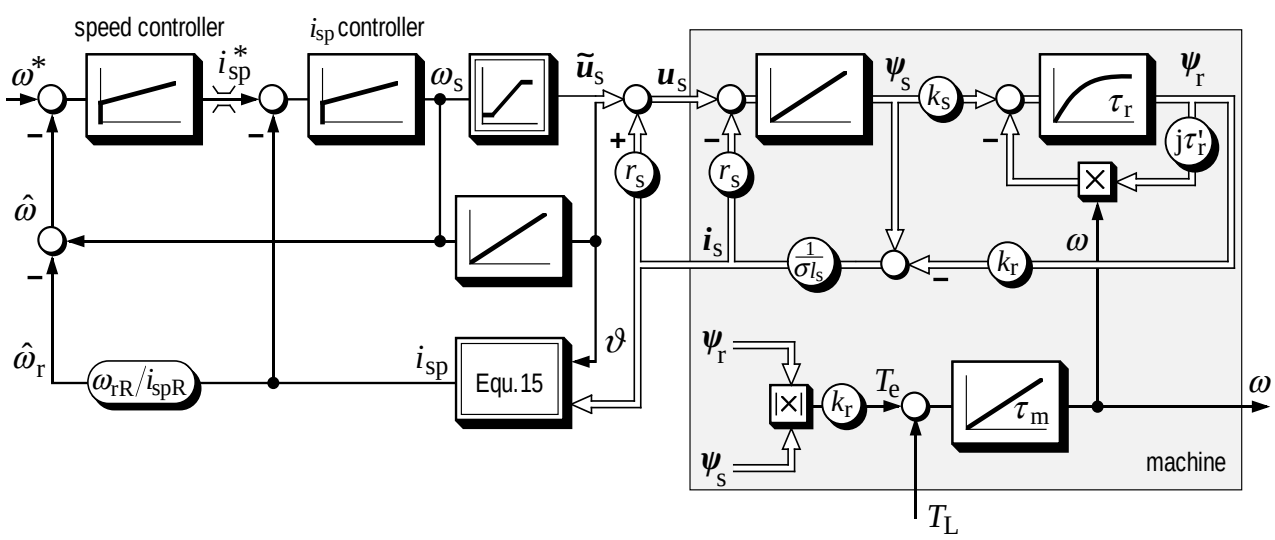

Fig. 4: Sensorless drive for moderate dynamic performance (subscript R: rated value)

By integrating the fundamental emf voltages measured at the stator winding taps, the airgap flux vector is estimated and made the basis of a field oriented control system. Owing to the low number of rotor slots, the speed resolution gets poor at low speed. This entails moderate speed control dynamics. However, the steady-state accuracy at higher speed is very good.

Saturation by the fundamental flux wave of the stator core also produces triplen harmonic stator emf components. This effect was studied by *Kreindler et al.* for sensorless speed control. Their paper [5] presents preliminary results.

V. High Performance Drives

5.1 Rotor field orientation

A fast current control system is usually employed to force the stator mmf distribution to any desired location and intensity in space, independent of the machine dynamics. The dynamic order then reduces, the system being now characterized by a single complex equation which is obtained from (1b) and (2). Referring to synchronous coordinates, $\omega_k = \omega_s$, we have

$$\tau_r \frac{d\boldsymbol{\psi}_r}{d\tau} + \boldsymbol{\psi}_r = -j\omega_r \tau_r \boldsymbol{\psi}_r + l_h \boldsymbol{i}_s, \tag{16}$$

where ω_r is the angular frequency of the induced rotor voltages. Fig. 5 shows that the stator current acts as the forcing function. It is commanded by the complex reference signal $\boldsymbol{i}_s^*$ of the current control loop.

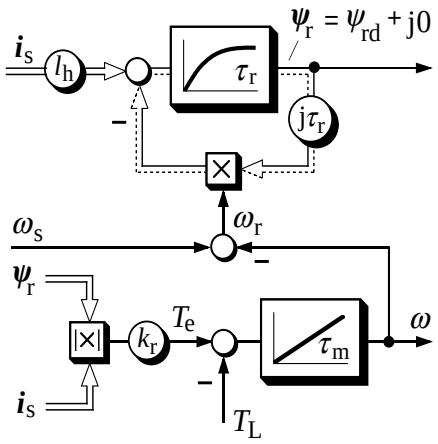

Fig. 5: Induction motor signal flow graph: forced stator currents. The dotted lines represent zero signals at rotor field orientation.

For dynamically decoupled control, all space vectors are referred to in a field oriented dq-coordinate system. Rotor field orientation defines the real axis be aligned with the rotor flux vector. The imaginary rotor flux component ψ_{rq} is then zero by definition, and all dotted signals in Fig. 5 assume zero values. The balance at the summing point in Fig. 5 defines the condition for rotor field orientation

$$l_h i_q = \omega_r \tau_r \psi_{rd}, \tag{17}$$

which can be satisfied by chosing ω_r appropriately. The signal flow diagram of the motor then assumes the familiar structure Fig. 6, permitting decoupled control of the machine torque.

Control by rotor field orientation requires on-line identification of the rotor flux vector since the rotor state variables cannot be directly measured in a squirrel cage machine. In a speed sensorless system, the speed signal as well must be obtained by estimation techniques.

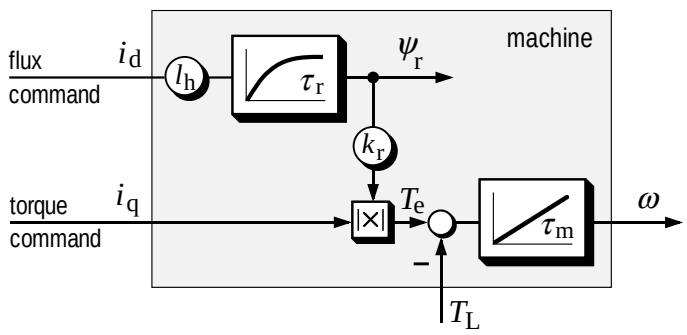

Fig. 6: Signal flow at rotor field orientation

5.2 Model reference adaptive system

The model reference approach (MRAS) makes use of the redundancy of two machine models of different structures that estimate the same state variable on the basis of different sets of input variables. The stator model in the upper portion of Fig. 7 serves as a reference model. Its equation is derived in the stationary reference frame, $\omega_k = 0$, from (1a) and (2)

$$\boldsymbol{\psi}_r = \int \left(\boldsymbol{u}_s - r_s \boldsymbol{i}_s - \sigma l_s \frac{d\boldsymbol{i}_s}{d\tau}\right) d\tau. \tag{18}$$

Its output is the estimated rotor flux vector $\hat{\boldsymbol{\psi}}_r$.

The rotor model equation is obtained from (1b) and (2) with reference to the stationary reference frame:

$$\tau_r \frac{d\boldsymbol{\psi}_r}{d\tau} + \boldsymbol{\psi}_r = j\omega \tau_r \boldsymbol{\psi}_r + l_h \boldsymbol{i}_s. \tag{19}$$

The model generates the rotor flux estimate from the measured stator current and from a tuning signal $\hat{\omega}$. The tuning signal is obtained through a PI controller from an error signal e, which represents the angular difference between the two estimated flux vectors. As the error signal e gets minimized, the tuning signal approaches the estimated speed $\hat{\omega}$. The rotor model as the adjustable model then produces the same rotor flux vector as the reference model.

Accuracy and drift problems that are inherent to the open integration in the reference model at low speed are alleviated by using a delay element instead of an integrator in the stator model Fig. 7. This makes the integration ineffective in the frequency range below $1/\tau_1$, and necessitates the addition of an equivalent bandwidth limiter for the adjustable rotor model. Below the cut-off frequency $1/\tau_1 \approx 1$ Hz, speed estimation becomes necessarily inaccurate. Even so, reversal of speed

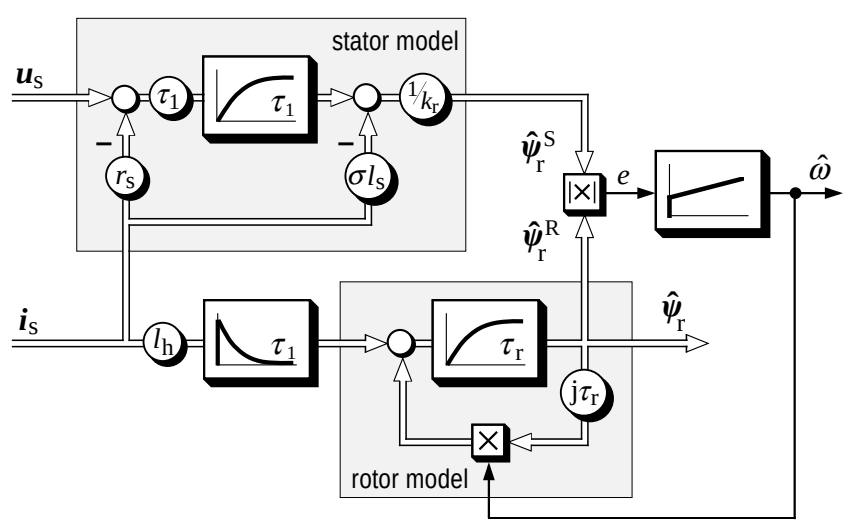

Fig. 7: Model reference adaptive system for speed estimation

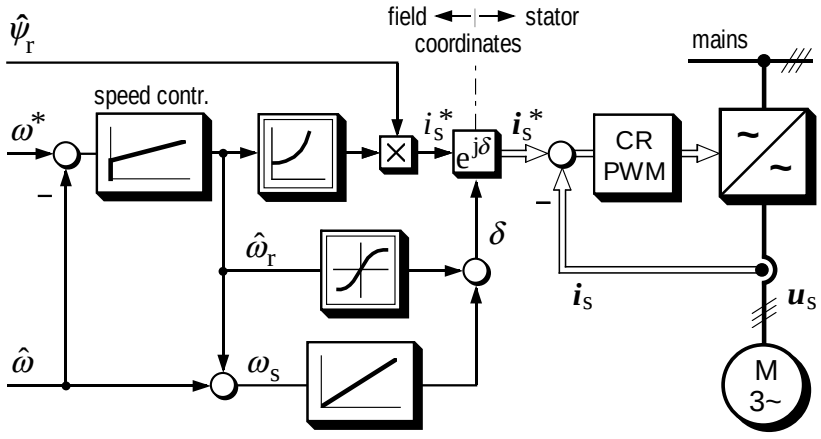

Fig. 8: Speed and current controller for MRAS estimator; CR PWM: current regulated pulsewidth modulator

through zero during a fast transient process is possible. However, if the drive is operated at zero stator frequency for more than a few seconds, the estimated flux goes astray and speed control is lost.

The speed control system is shown in Fig. 8. The speed estimate $\hat{\omega}$ is supplied by the model reference adaptive system Fig. 7. The speed controller generates a rotor frequency signal $\hat{\omega}_r$, which controls the stator current magnitude

$$i_s = \frac{\psi_{rd}}{l_s}\sqrt{1+\hat{\omega}_r^2\,\tau_r^2}\ , \qquad (20)$$

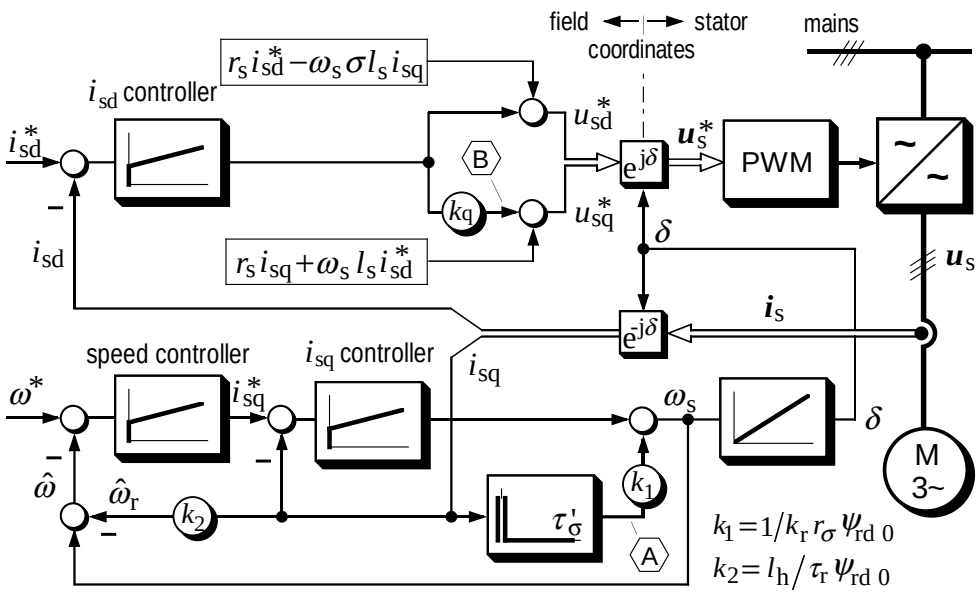

Fig. 9: Feedforward control of stator voltages, rotor flux orientation

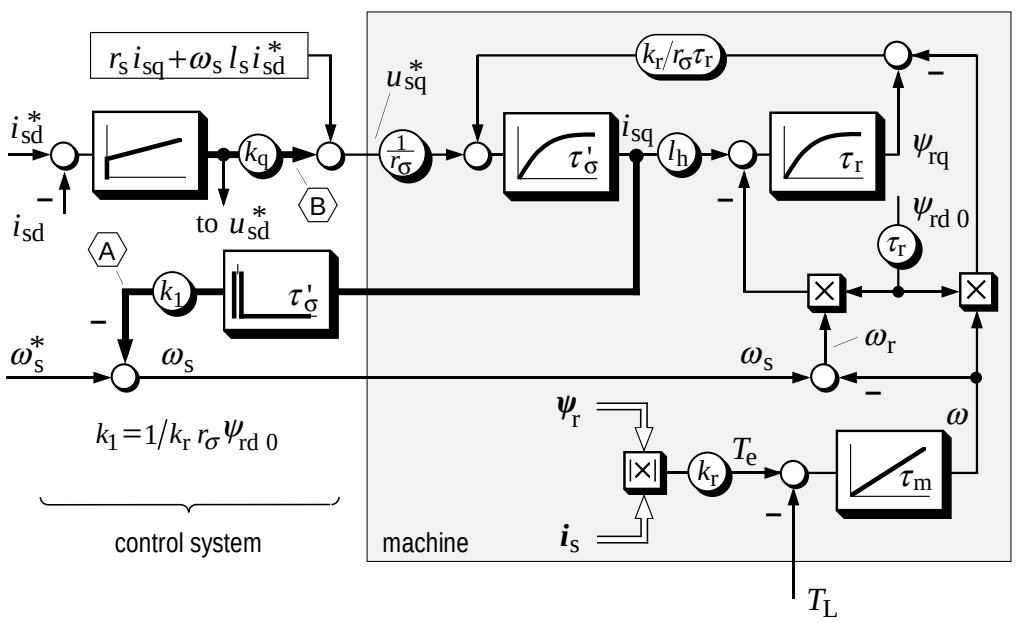

Fig. 10: Compensation channels (thick lines at *A* and *B*) for the speed sensorless control system Fig. 9

and its phase angle

$$\delta = \int \omega_s\, d\tau + tan^{-1}(\hat{\omega}_r \tau_r). \qquad (21)$$

Equations (20) and (21) are derived from (17) and from the steady-state solution $i_{sd} = \psi_{rd}/l_h$ of (19) in field coordinates.

It is a particular feature of this approach that, provided the same value of τ_r is used in the rotor model and in the control functions (20) and (21) of the speed control system Fig. 8, accurate orientation of the injected current vector is achieved even if value of τ_r differs from the actual rotor time constant of the machine. If the tuning controller in Fig. 7 maintains nearly zero error, the rotor model exactly replicates that dynamic relationship between the stator current vector and the rotor flux vector which exists in the actual motor [6]. However, the accuracy of speed estimation, reflected in the feedback signal $\hat{\omega}$ to the speed controller, does depend on the error in τ_r. Parameter mismatch of the reference model is another source of inaccuracy.

Good dynamic performance of the system is reported by *Schauder* above 2 Hz stator frequency [6].

5.3 Feedforward Control of Stator Voltages

In the approach of *Okuyama et al.* [7], the stator voltage reference in field coordinates, $\boldsymbol{u}_s^{*(F)}$, is basically generated as a feedforward signal. The components of this signal are derived from (4a) under the assumption of steady-state conditions, $d/d\tau \approx 0$, from which $\psi_{rd} = l_h\, i_{sd}$ follows, and using the approximation $\omega \approx \omega_s$:

$$u_{sd} = r_\sigma i_{sd} - \omega_s\, \sigma l_s\, i_{sd} \qquad (22a)$$

$$u_{sq} = r_\sigma i_{sq} + \omega_s\, l_s\, i_{sd} \qquad (22b)$$

The *d*-axis current i_{sd} is replaced by its reference value i_{sd}^*. The resulting feedforward signals are represented by the framed equations in Fig. 9. The signals depend on machine parameters, which creates the need for error compensation by a superimposed control loop. An i_{sd} controller ensures primarily the error correction of u_{sd}^*, thus governing the machine flux. The signal i_{sq}^*, which represents the torque reference, is obtained as the output of the speed controller. The speed estimate $\hat{\omega}$ is composed of the stator frequency ω_s and the estimated the rotor frequency $\hat{\omega}_r$; the latter is proportional to the torque building current i_{sq}. Since the torque increases when the velocity of the revolving field is increased, ω_s and hence the field angle δ can be derived from the i_{sq} controller.

Although the system so far described is equipped with controllers for both stator current components, i_{sq} and i_{sq}, the internal cross-coupling between the input variables and the output variables of the machine is not eliminated under dynamic conditions. This means that the desired decoupled machine structure of Fig. 5 is not realized. The reason is that the *q*-axis current gets only indirectly controlled through acceleration or deceleration of the rotating reference frame.

To demonstrate this, the dynamic behavior of the machine is modelled by studying the signal flow graph

Fig. 1 for small deviations from the state of correct field orientation. The reduced flow graph Fig. 10 shows that the d-axis rotor flux is then constant, denoted as $\psi_{\mathrm{rd}\,0}$, while nonzero q-axis rotor flux indicates a deviation. It is now assumed that the mechanical speed ω changes. A decrease of ω, for instance, increases ω_r and hence produces negative $d\psi_\mathrm{rq}/d\tau$. Simultaneously, the component $-k_\mathrm{r}\,\omega\psi_{\mathrm{rd}\,0}$ of the q-axis back-emf, which acts on the stator winding through the machine coefficient $k_\mathrm{r}/r_\sigma\tau_\mathrm{r}$ in Fig. 10, is increased. Then i_r rises, delayed by τ_sr', and restores $d\psi_\mathrm{rq}/d\tau$ to zero after some time. Before that, ψ_rq has assumed a nonzero value, and field orientation is lost.

A similar effect occurs on a change of ω_s^* which instantaneously affects $d\psi_\mathrm{rq}/d\tau$, while this disturbance is cancelled only after a delay of τ_sr' by the feedforward adjustment of u_sq through ω_s.

Both undesired perturbations are eliminated by the addition of a signal proportional to $-di_\mathrm{sq}/d\tau$ to the stator frequency input of the machine controller. This compensation is marked *A* in Fig. 9 and Fig. 10.

The mechanism of maintaining field orientation needs further explanation. In the dynamic structure Fig. 1, the signal $-\mathrm{j}\omega\tau_\mathrm{r}\boldsymbol{\psi}_\mathrm{r}$, which essentially contributes to the back-emf vector, influences upon the stator current derivative. A misalignment between the reference frame and the rotor flux vector produces a nonzero ψ_rq value, giving rise to a back-emf component that changes i_sd. Since the feedforward control of u_sd^* is determined by (22a) on the assumption of existing field alignment, this deviation will invoke a correcting signal from the i_sd controller. The signal is made to influence, through a gain constant k_q, upon the quadrature voltage u_sq^* (channel *B* in Fig. 9 and Fig. 10) and hence on i_sq as well, causing the i_sq controller to accelerate or decelerate the reference frame to reestablish accurate field alignment.

Torque rise time of this scheme is reported around 15 ms; speed accuracy is within ± 1% above 3% rated speed and ± 12 rpm at 45 rpm [5].

5.4 Estimation of rotor flux and torque current

A sensorless rotor flux orientation scheme based on the stator model is described by *Ohtani* [8]. The upper portion of Fig. 11 shows the classical structure in which controllers for

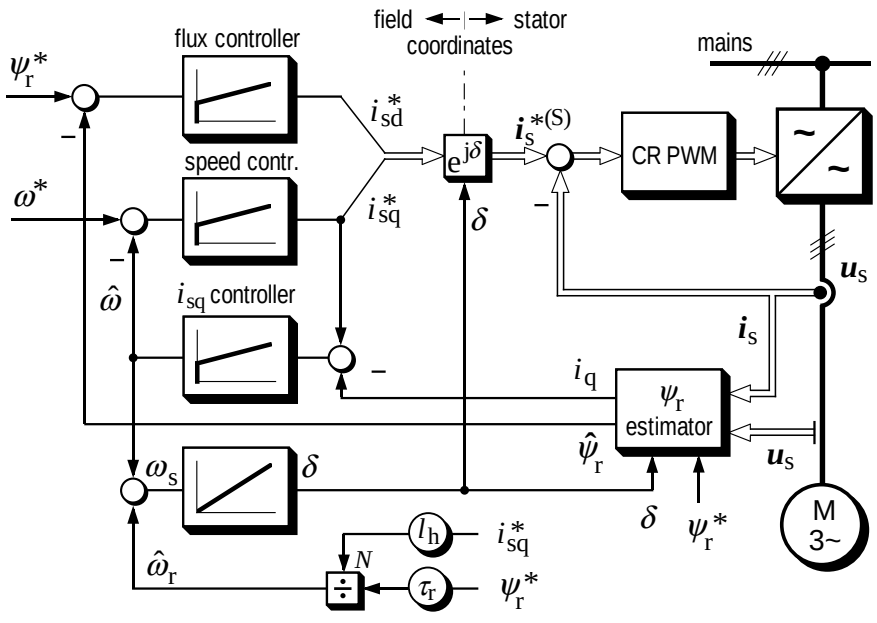

Fig. 11: Speed sensorless control based on direct i_sq estimation, rotor field orientation

speed and rotor flux, respectively, generate the current reference vector $\boldsymbol{i}_\mathrm{s}^* = i_\mathrm{sd}^* + \mathrm{j}\,i_\mathrm{sq}^*$ in field coordinates. This signal is transformed into stator coordinates and handled by a set of fast current controllers. Possible misalignment of the reference frame is detected as the difference of the measured q-axis current from its reference value i_sq^*. This error signal feeds a PI controller, the output of which is the estimated mechanical speed $\hat{\omega}$. It is added to an estimate $\hat{\omega}_\mathrm{r}$ of the rotor frequency, computed from the reference values i_sq^* and ψ_r^*. Integration of ω_s provides the field angle δ.

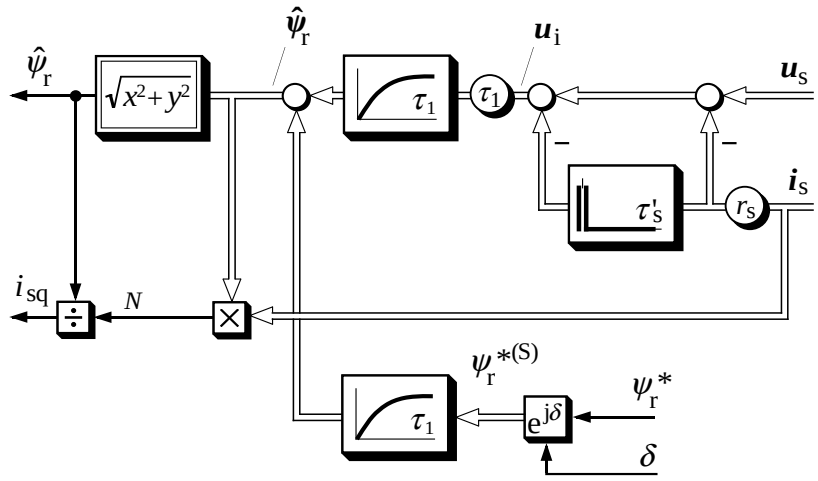

Fig. 12: Rotor flux estimator for the structure Fig. 10

The estimation of the rotor flux vector $\boldsymbol{\psi}_\mathrm{r}$ is based on the stator model. From (1a) and (2) we obtain the equation

$$\tau_1 \frac{d\boldsymbol{\psi}_\mathrm{r}}{d\tau} + \boldsymbol{\psi}_\mathrm{r} = \tau_1\left(\boldsymbol{u}_\mathrm{s} - r_\mathrm{s}\boldsymbol{i}_\mathrm{s} - r_\mathrm{s}\tau_\mathrm{s}'\frac{d\boldsymbol{i}_\mathrm{s}}{d\tau}\right), \qquad (23)$$

which is solved in stator coordinates using measured values of the terminal currents and voltages. Fig. 12 shows the signal flow scheme. The drift problems of an open integration at low frequency are by-passed by a band-limited integration of the high-frequency components, while replacing the inaccurate estimation of $\boldsymbol{\psi}_\mathrm{r}$ at stator frequencies below $1/\tau_1$ by the reference value $\boldsymbol{\psi}_\mathrm{r}^*$ in a smooth transition. Hence $\boldsymbol{\psi}_\mathrm{r} \approx \boldsymbol{\psi}_\mathrm{r}^*$ at lower frequencies, which means that the flux controller is virtually deactivated. However, its last output signal i_sd^* is maintained during low speed operation, and so is the rotor flux magnitude. Nevertheless, field orientation may be lost at very low stator frequency. Closed loop rotor flux control is resumed as soon as the speed increases again.

Note that the q-axis current is directly taken as the current component in quadrature with the estimated rotor flux vector. It carries the original information on the field angle at higher speed. The i_sq-controller then adjusts the estimated speed, and in consequence the field angle at which the stator current is injected by the inverter control.

At 18 rpm, speed accuracy is reported to be within ± 3 rpm. Torque accuracy at 18 rpm is about ± 0.03 pu. at 0.1 pu. reference torque, improving significantly as the torque increases. Minimum parameter sensitivity exists at $\tau_1 = \tau_\mathrm{r}$ [8].

5.4 Stator flux orientation

An alternative approach in sensorless control is the orientation of the synchronous reference frame to the stator flux vector. Employing fast stator current control makes the stator current vector the forcing function, and a complex first-order system results in which the stator flux vector is a state varia-

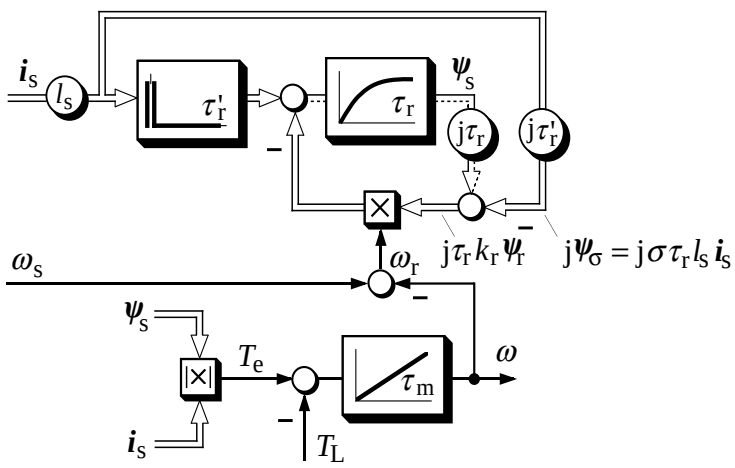

Fig. 13: Induction motor signal flow graph, forced stator curents; state variables: stator current, stator flux. The dotted lines represent zero signals at stator field orientation.

ble. The machine equation is obtained from (16) and (2),

$$\tau_r \frac{d\boldsymbol{\psi}_s}{d\tau} + \boldsymbol{\psi}_s = -j\omega(\tau_r \boldsymbol{\psi}_s - \tau_r' l_s \boldsymbol{i}_s) + \tau_r' l_s \frac{d\boldsymbol{i}_s}{d\tau} + l_s \boldsymbol{i}_s, \qquad (24)$$

which defines the signal flow graph Fig. 13. This structure is less straightforward than its equivalent at rotor flux orientation, Fig. 5. The condition for stator flux orientation, $\psi_{sq} = 0$, can be read from the balance at the upper summing point in Fig. 13

$$l_s\left(\tau_r' \frac{di_{sq}}{d\tau} + i_{sq}\right) = \omega_r \tau_r \left(\psi_{sd} - \sigma l_s i_{sd}\right), \qquad (25)$$

taking into account that the dotted lines represent signals of zero magnitude at stator flux orientation. The dynamic structure is then simplified as shown in the shaded area of Fig. 14.

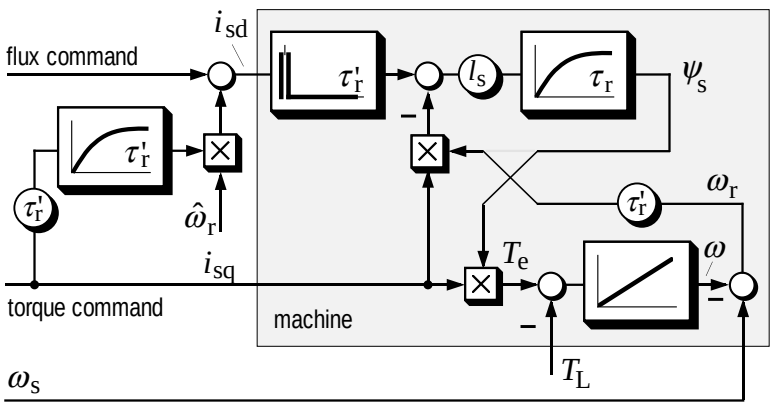

Fig. 14: Machine control at stator flux orientation using an external dynamic decoupler

The torque command has now an undesired influence on the stator flux. *Xu et al* [9] propose a decoupling arrangement, shown in the left of Fig. 14, to eliminate the cross-coupling between the *q*-axis current and the stator flux. The decoupling signal depends on the rotor frequency, which is estimated based on (25):

$$\hat{\omega}_r = \frac{l_s}{\tau_r} \frac{\tau_r' \dfrac{di_{sq}}{d\tau} + i_{sq}}{\psi_{sd} - \sigma l_s i_{sd}}. \qquad (26)$$

Fig. 14 shows that the internal influence of i_{sq} is cancelled by the external decoupling signal.

The angular mechanical velocity can be expressed as

$$\hat{\omega}_s = \frac{d\delta}{d\tau} = \frac{d}{d\tau}\left(tan^{-1}\left(\frac{\psi_{sq}}{\psi_{sd}}\right)\right), \qquad (27)$$

from which

$$\hat{\omega}_s = \frac{1}{\psi_s^2} \cdot \left| \boldsymbol{\psi}_s \times \frac{d\boldsymbol{\psi}_s}{d\tau} \right|_z \qquad (28)$$

is obtained. The stator flux vector $\boldsymbol{\psi}_s$ is generated by open integration. Fig. 15 shows the signal flow schematic. Drift and accuracy problems are minimized by employing a fast signalprocessor, selfcalibrating A/D converters of high sampling rates, and automated parameter initialization [10]. Smooth operation is achieved at 30 rpm with rated load torque.

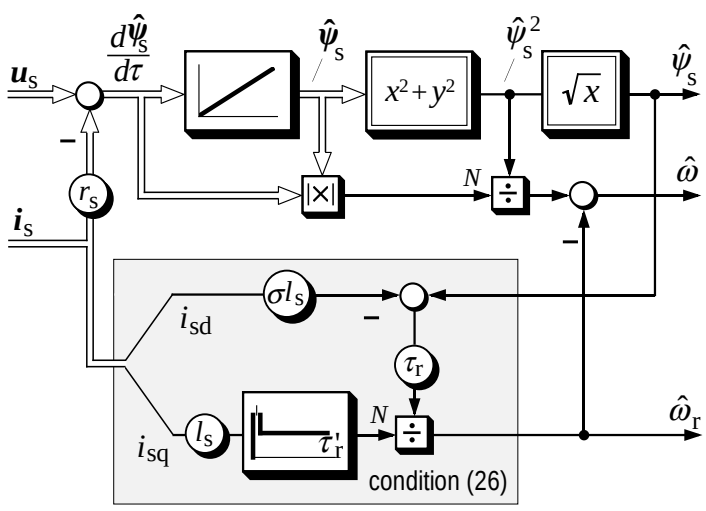

Fig. 15: Speed and rotor frequency estimator for control of the system Fig. 14; *N*: Numerator

VI. Adaptive Observers

The accuracy of the open loop estimation models described in the previous chapter reduces as the mechanical speed reduces. The limit of acceptable performance depends on how precisely the model parameters can be matched to the corresponding parameters in the actual machine. It is particularly at lower speeds that parameter deviations have significant influence on the steady-state and dynamic performance of the drive system.

The robustness against parameter mismatch and signal noise can be improved by employing closed loop observers for the estimation of the state variables, and possibly of the

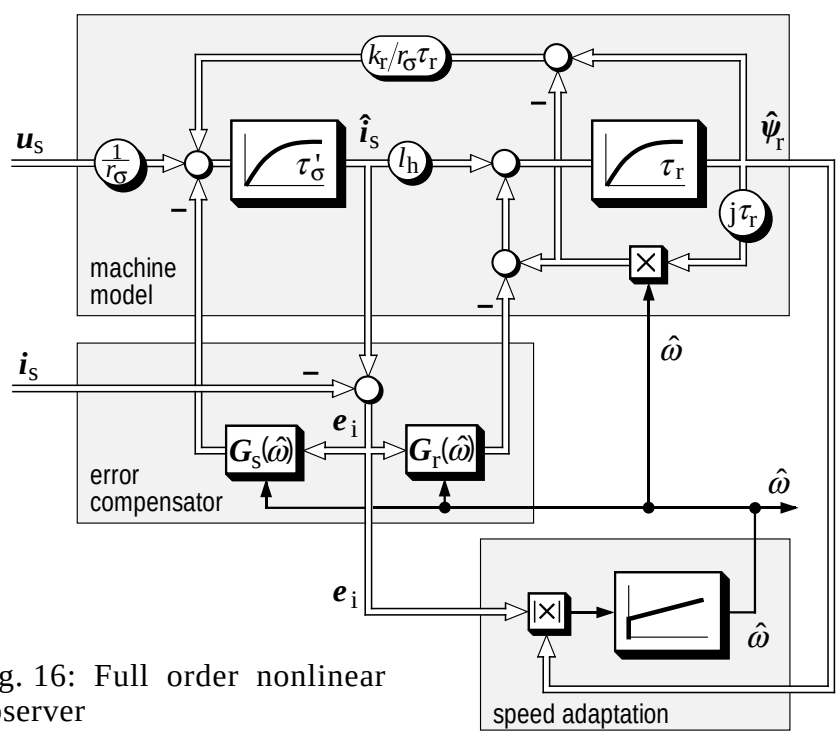

Fig. 16: Full order nonlinear observer

system parameters.

6.1 Full order nonlinear observer

A full order observer can be constructed from the machine equations (4). The stationary coordinate system is chosen, $\omega_k = 0$, from which the machine model in the upper frame in Fig. 16 results.

Adding an error compensator to the model establishes the observer. The error between the model current and the machine current is $\boldsymbol{e}_i = \hat{\boldsymbol{i}}_s - \boldsymbol{i}_s$. It is used to generate corrective inputs to the dynamic subsystems of the stator and the rotor, which yields the observer equations from (4):

$$\tau_\sigma' \frac{d\boldsymbol{i}_s}{d\tau} + \boldsymbol{i}_s = -j\omega_k \tau_\sigma' \boldsymbol{i}_s + \frac{k_r}{r_\sigma \tau_r}(1 - j\omega\tau_r)\boldsymbol{\psi}_r + \frac{1}{r_\sigma}\boldsymbol{u}_s - \boldsymbol{G}_r(\hat{\omega})\boldsymbol{e}_s \qquad (29a)$$

$$\tau_r \frac{d\boldsymbol{\psi}_r}{d\tau} + \boldsymbol{\psi}_r = -j(\omega_k - \omega)\tau_r \boldsymbol{\psi}_r + l_h \boldsymbol{i}_s - \boldsymbol{G}_r(\hat{\omega})\boldsymbol{e}_s \qquad (29b)$$

Kubota et al. [11] select the complex gain factors $\boldsymbol{G}(\hat{\omega})$ such that the two complex eigenvalues of the observer $\boldsymbol{\lambda}_{1,2\ obs} = k \cdot \boldsymbol{\lambda}_{1,2\ mach}$, where $\boldsymbol{\lambda}_{1,2\ mach}$ are the machine eigenvalues, and $k > 1$ is a real constant. The value of k scales the observer by pole placement to be dynamically faster than the machine. Given the nonlinearity of the system, the resulting complex gains $\boldsymbol{G}_s(\hat{\omega})$ and $\boldsymbol{G}_r(\hat{\omega})$ in Fig. 16 depend on the the estimated angular mechanical speed $\hat{\omega}$ [11].

The signal $\hat{\omega}$ is also required to adapt the rotor structure of the observer to the mechanical speed of the machine. The signal is obtained through a PI controller, primarily from the current error $\boldsymbol{e}_i$. More specifically, the term $|\boldsymbol{\psi}_r \times \boldsymbol{\varepsilon}_i|_z$ represents the torque error. It is computed to include also the sign of the deviation between the estimated speed and the actual speed. Minimum speed is reported as 0.034 p.u. or 50 rpm.

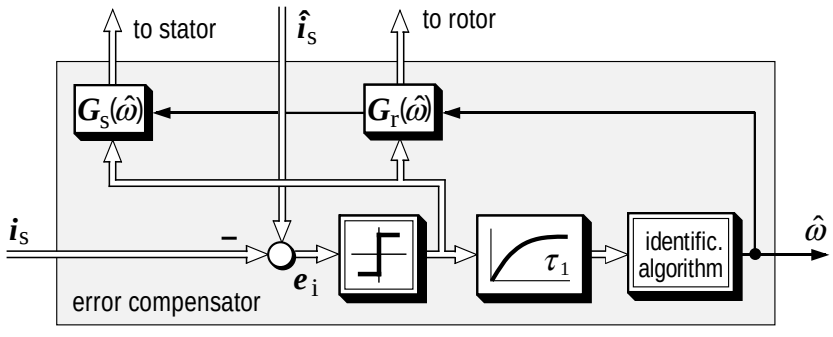

Fig. 17: Sliding mode compensator. The compensator is interfaced with the machine model Fig. 16 to form a sliding mode observer

6.2 Sliding mode observer

The effective gains of the error compensator can be increased by using a sliding mode controller to tune the observer for speed adaptation and for rotor flux estimation. This method is proposed by *Sangwongwanich* and *Doki* [12]. Fig. 17 shows the dynamic structure of the error compensator. It is interfaced with the machine model the same way as the error compensator in Fig. 16.

In the compensator, the current error vector $\boldsymbol{e}_i$ is used to define the sliding hyperplane. The estimation error is then forced to zero by a high-frequency nonlinear switching controller. The switched waveform can be directly used to exert a compensating influence on the machine model, while its average value controls an algorithm for speed identification. The robustness of the sliding mode approach ensures zero error of the estimated stator current. The H_∞-approach is used for pole placement in observer design to minimize the rotor flux error in the presence of parameter deviations. The practical implementation requires a fast signalprocessor. The authors have operated the system at 0.036 p.u. minimum speed.

6.3 Extended Kalman filter

Kalman filtering techniques can be based on the complete machine model, which is the same as shown in the upper frame in Fig. 16. The machine is modelled as a 5th-order system, introducing the mechanical speed as an additional state variable. Since the model is nonlinear, the extended Kalman algorithm must be applied. It linearizes the nonlinar model in the actual operating point. The corrective inputs to the dynamic subsystems of the stator, the rotor, and the mechanical model are derived such that a quadratic error function is minimized. The error function is evaluated on the basis of predicted state variables, taking into account the noise in the measured signals and in the model parameter deviations. The statistical approach reduces the error sensitivity, permitting also the use of models of lower order than the machine.

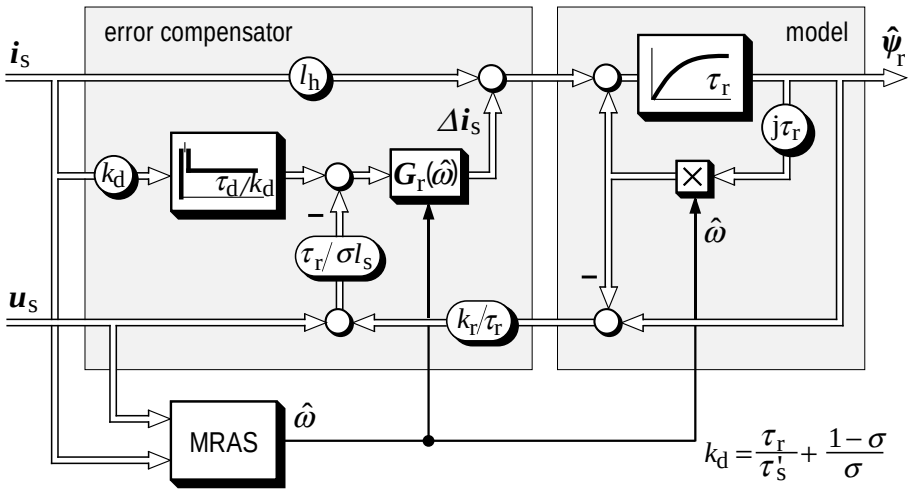

Fig. 18: Reduced order nonlinear observer; the MRAS block contains the structure Fig. 7.

Henneberger et al. [13] have reported an experimental verification of this method using machine models of 4th and 3rd order. This relaxes the extensive computation requirements to some extent; the implementation, though, requires floating-point signalprocessor hardware.

6.4 Reduced order nonlinear observer

Hori et al. [14] use a nonlinear observer of reduced dynamic order for the identification of the rotor flux vector.

The model, shown in the right-hand side frame in Fig. 18, is a complex first order system based on the rotor equation (8). It receives the measured stator current vector as an input signal. The error compensator, shown left, generates an additional model input

$$\Delta\boldsymbol{i}_s = \boldsymbol{G}_r(\hat{\omega}) \begin{bmatrix} \tau_r \frac{d\boldsymbol{i}_s}{d\tau} + \left(\frac{\tau_r}{\tau_s'} + \frac{1-\sigma}{\sigma}\right)\boldsymbol{i}_s \\ -\frac{\tau_r}{\sigma l_s}\left(\boldsymbol{u}_s + \frac{k_r}{\tau_r}(1 - j\omega\tau_r)\boldsymbol{\psi}_r\right) \end{bmatrix} \qquad (30)$$

which can be interpreted as a stator current component that reduces the influence of model parameter errors. The field transformation angle δ as obtained from the reduced order observer is independent of rotor resistance variations [14]. The complex gain $\boldsymbol{G}_r(\hat{\omega})$ ensures fast dynamic response of the observer by pole placement. The reduced order oberserver employs a model reference adaptive system as in Fig. 5 as a subsystem for the estimation of the rotor speed. The estimated speed is used as a model input.

VII. Comparison

Controlled induction motor drives without speed sensor extract information on the mechanical shaft speed from measured stator voltages and currents at the motor terminals. The majority of speed identification methods rely on the approximated fundamental model of the machine. The use of the stator equation, particularly the integration of the stator voltage vector, is common for all methods. Its solution is fairly accurate when the switched stator voltage waveform is measured at high bandwidth, and when the parameters that determine the contributions of the resistive and the leakage voltage components are well known. As the influence of these parameters dominates the estimation at lower speed, the steady-state accuracy of speed sensorless operation tends to be poor in the low speed range. The dynamic performance depends on the accuracy of field angle estimation, which is also parameter dependent.

Robust estimation techniques and parameter identification by self-commissioning or by on-line tuning have the potentiality of reducing the estimation errors. The limit of tolerable performance can be then extended to lower speed levels; stable operation at zero stator frequency, though, is not possible with the fundamental model of the machine, which then becomes unobservable. However, a fast reversal of speed through the point of zero stator frequency is not a problem with most methods. Hence the benefit of reducing the lower speed limit by more sophisticated identification techniques may not always appear worthwhile for many applications.

The graph Fig. 19 gives a comparison of different methods for speed sensorless control in terms of the torque rise time t_r and the low speed limit of stable operation. The data has been taken from the cited references; it should be considered approximate, since the individual test und evaluation conditions may differ. The steady-state speed accuracy at the lower speed limit depends on the accurate setting of the model parameters and hence varies with parameter drift.

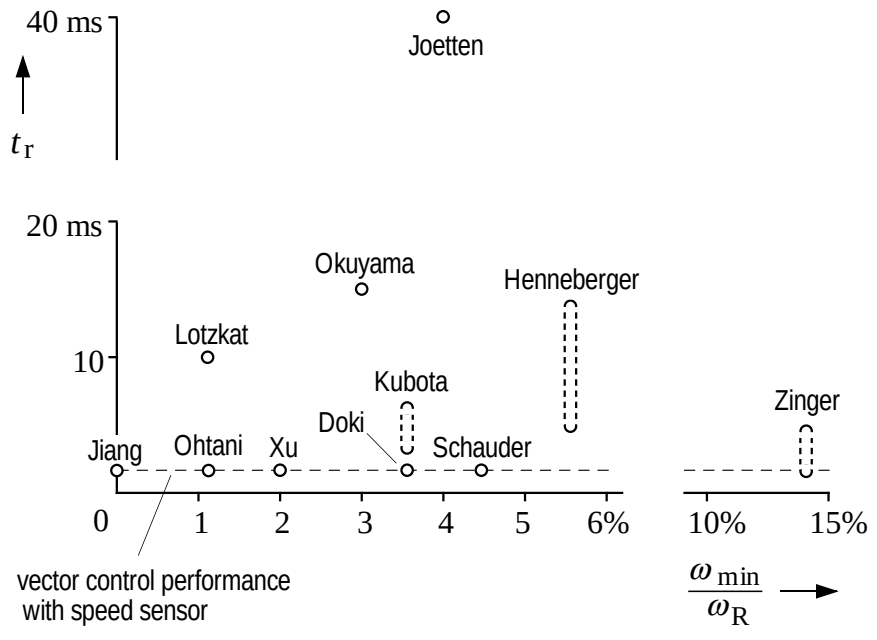

Fig. 19: Performance comparison of speed sensorless drive control methods

VIII. Summary

Controlled ac drives without mechanical sensors for speed or motor shaft position have the attraction of lower cost and higher reliability. A variety of sensorless controlled ac drive schemes are available for practical application. Speed estimators are used for moderate dynamic requirements. High-performance vector control requires a flux vector estimator in addition. The robustness of a sensorless ac drive can be improved by adequate control structures and by parameter identification techniques. Depending on the respective approach, sensorless control can be achieved over a base speed range of 1:100 to 1:150 at very good dynamic performance. Preference for industrial application will certainly be given to algorithms that can be implemented in standard microcontroller hardware.

IX. References

1. J. Holtz, „The Representation of AC Machine Dynamics by Complex Signal Flow Graphs", *IEEE Trans. Ind. Electronics*, Vol 42, No. 3, June 1995, pp. 263-271.
2. R. Jötten und G. Maeder, „Control Methods for Good Dynamic Performance Induction Motor Drives Based on Current- and Voltage as Measured Quantities", *IEEE Trans. Industry Appl.*, Vol-IA-19, No. 3, 1983, pp. 356-363.
3. W. Lotzkat, „Industrial Low-Cost PWM Inverter Drives with Ride-Through Capability", *Ph.-D Thesis* (in German), 1991, Wuppertal University.
4. D. Zinger, F. Profumo, T. A. Lipo, and D. W. Novotny, „A Direct Field-Oriented Controller for Induction Motor Drives Using Tapped Stator Windings", *IEEE PESC 1988 Record*, pp. 855-861.
4. L. Kreindler. J. C. Moreira, A. Testa, and T. A. Lipo, „Direct Field-Orientation Controller Using the Stator Phase Voltage Third Harmonic", *IEEE IAS Ann. Meet.*, 1992, pp. 508-514.
5. C. Schauder, „Adaptive Speed Identification for Vector Control of Induction Motors without Rotational Transducers", *IEEE IAS Ann. Meet.*, 1989, pp. 493-499.
7. T. Okuyama, N. Fujimoto, T. Matsui und Y. Kubota, „A High Performance Speed Control Scheme for Induction Motor without Speed and Voltage Sensors", *IEEE IAS Ann. Meet.*, 1986, pp. 106-111.
8. T. Ohtani, N. Takada, and K. Tanaka, „Vector Control of Induction Motor without Shaft Encoder", *IEEE Trans. Industry Appl.*, Vol. 28, No. 1, 1992, pp. 157-165.
9. X. Xu, D. W. Novotny, „Implementation of Direct Stator Flux Oriented Control on a Versatile DSP Based System", *IEEE Trans. Industry Appl.*, Vol. 29, No. 2, 1991, pp. 694-700.
10. J. Holtz, A. Khambadkone, „Vector Controlled Induction Motor Drive with a Self-Commissioning Scheme", *IEEE Trans. Ind. Electronics*, 1991, pp. 322-327.
11. H. Kubota, K. Matsuse, and T. Nakano, „DSP Based Speed Adaptive Flux Observer of Induction Motor", *IEEE Trans. Industry Appl.*, Vol. 29, No. 2, 1993, pp. 344-348.
12. S. Doki, S. Sangwongwanich, T. Yonemoto, and S. Okuma, „Implementation of Speed-Sensorless Field-Oriented Vector Control Using Adaptive Sliding Observers", *IECON, 16th Ann. Conf. of the IEEE Industrial Elect. Soc.*, Asilomar/Ca., 1990, pp. 453-458.
13. G. Henneberger, B. J. Brunsbach, and Th. Klepsch, „Field Oriented Control of Synchronous and Asynchronous Drives without Mechanical Sensors Using a Kalman-Filter", *Europ. Conf. Power Electr. and Appl. EPE*, Florenz 1991, pp. 3/664-671.
14. H. Tajima, Y. Hori, „Speed Sensor-Less Field-Orientation Control of the Induction Machine", *IEEE Trans. Industry Appl.*, Vol. 29, No. 1, 1993, pp. 175-180.